Designing an illegal mining detection system based on DInSAR

Author:
Hu, Z; Ge, L; Li, X; Rizos, C; Li, Xiaojing

Publication details:
IGARSS 2010: IEEE International Geoscience and Remote Sensing Symposium
pp. 3952 - 3955
9781424495665 (ISBN)
2153-6996 (ISSN)

Event details:
30th IEEE International Geoscience and Remote Sensing Symposium, IGARSS 2010
Honolulu, HI, USA
2010-07-25 - 2010-07-30

Publication Date:
2010-01-01

Publisher DOI:
https://doi.org/10.1109/igarss.2010.5652978

DESIGNING AN ILLEGAL MINING DETECTION SYSTEM BASED ON DINSAR

Zhe Hu, Linlin Ge, Xiaojing Li and Chris Rizos

Cooperative Research Centre for Spatial Information & School of Surveying and Spatial Information Systems,
the University of New South Wales, Sydney, NSW, 2052, Australia

ABSTRACT

Satellite Differential Radar Interferometry (DInSAR) has demonstrated its ability for monitoring mine-induced ground subsidence. However, it is still a challenging task to routinely identify all mining activities from the large-scale coverage interferogram, especially the illegal mines. In response to this challenge an underground mining detection system based on DInSAR is described. The system is tested over a dense mining area in Asia. With such a system it is hoped that the detection efficiency of illegal underground mining using DInSAR can be improved.

Index Terms— Differential SAR Interferometry, Underground Mining Detection, Deformation Gradient

1. INTRODUCTION

Ground subsidence is a serious threat to surface facilities, infrastructure, buildings, real estate or even human lives. This phenomenon is considerably worse in underground mining areas as excavation of minerals, etc., reduces the support of the ground surface above the mine area. Close monitoring therefore must be maintained in order to predict and/or minimise the impacts of land subsidence. The task can be generally be undertaken by using ground surveying methods, such as digital levels, total stations and global positioning system (GPS) techniques. However, in the case of illegal underground mining such techniques are inadequate because the locations of the mining are (in general) not known. In this case, satellite Differential Radar Interferometry (DInSAR) could be used to monitor mining across a large region.

The satellite DInSAR technique has demonstrated its advantages and capability of monitoring land subsidence caused by underground mining activities, as reported in [1] and [2]. Compared to traditional surveying methods it is able to simultaneously satisfy the goals of high accuracy and large coverage. Meanwhile, recent developments in relation to Synthetic Aperture Radar (SAR) satellites ensure that there will be sufficient data for long term surveillance. To obtain the monitoring result, a raw interferogram image is first generated, in order to estimate the ground deformation patterns. It is obtained by calculating the phase (travel time) difference of radar echoes between the SAR satellite's two passes over the same area, separated by multiples of the satellite repeat period. Then, the topographic phase contribution to the raw interferogram is removed, with the residual phase (differential interferogram) mostly attributable to ground deformation. If the magnitude of deformation is required, a few subsequent processes will be implemented, such as phase unwrapping [3], obtaining the spatial deformation signature between two SAR image acquisitions from the interferogram.

Thanks to the large-scale coverage of SAR images, the mining status and mine site locations over the whole region can be easily extracted from DInSAR results. However, it is challenging to locate all illegal mines across a vast region using manual processes. To deal with this problem, an Illegal Mining Detection System (IMDS) is proposed in this paper. A demonstration of the IMDS will illustrate the performance of this system.

2. SYSTEM DESIGN AND METHODOLOGY

2.1. Principle of Illegal Mine Detection

In order the locate mines from a DInSAR interferogram, the unique attributes of the mining subsidence and its pattern in the interferogram can be utilised. A typical pattern due to mining subsidence is also shown in Figure 1.

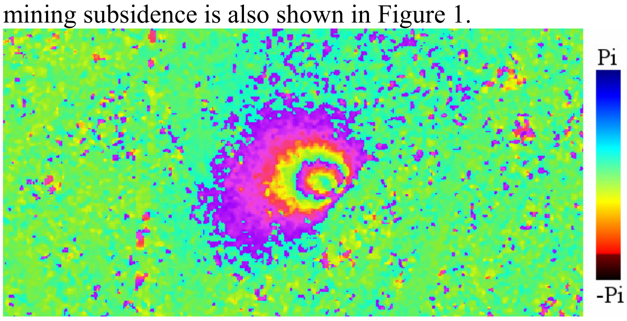

Figure 1. Typical pattern of mining subsidence in an DInSAR interferogram

A. The first obvious characteristic is that the deformation due to mining is that the surface under which mining occurs will sink (shown in Figure 1 as the colour of the subsidence fringes changing from purple to red). The greatest subsidence mostly occurs in the surface centre of underground mining activities, and the subsidence magnitude decreases from centre to edge, finally forming a spatial funnel in the area.

B. Another characteristic that can be deduced from attribute A is that since the deformation typically has a funnel shape, the mining centre is surrounded by slopes. It also means that the absolute values of the deformation gradient near the centre should be larger than the area where there is no deformation occurring. Meanwhile, the directions of the gradient are approximately pointing outside the pattern with reverse extensions to the subsidence centre. The 2D gradient is expressed as a complex number, where the magnitude represents the strength of the gradient and the phase indicates its direction:

$$\nabla f(x,y) = \frac{\partial f(x,y)}{\partial x} + i\frac{\partial f(x,y)}{\partial y} \tag{1}$$

C. Also, as shown in Figure 1, it can be concluded that the pattern is typically a round or oval shape. This is because the land surface can generally be considered as elastic [4], which means that the deformation spreads stably from the centre. Consequently the contours of deformation fringes represent a closed circle in the DInSAR's line-of-sight (LOS) direction.

Based on these attributes it is possible to distinguish the patterns of subsidence due to underground mining from DInSAR results, and locate their positions automatically. The processes are described in the following section.

2.2. Processing Flow of Automatic Detection

The detailed processing flow of IMDS is illustrated in Figure 2, consisting of six modules.

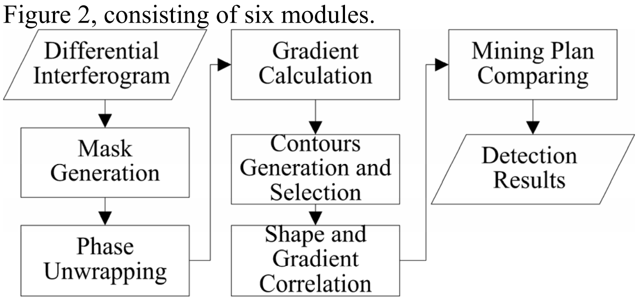

Figure 2. Processing flow of the IMDS

The most important module of IMDS's initial steps is *Phase Unwrapping*, which is used to obtain the absolute deformation values from the differential interferogram. It is also a precondition to evaluate whether Attribute A is satisfied or not. In order to obtain a high quality unwrapped result, use of a mask is necessary [5]. It is used to block out the areas that may induce errors in the result. As illustrated in Figure 2, the *Mask Generation* module is therefore the first to be implemented, right before the *Phase Unwrapping* module.

The objective of *Mask Generation* identifies the areas with dense residual points, which are too noisy and include DEM (Digital Elevation Model) errors, and these will not be unwrapped. In this paper, the determination of residual point is done by examining if there is over $\pm\pi$ phase change between nearby points. Then, a moving window is adopted to check the density of the residual points. The block with high density (over the predefined threshold) will be treated as the masked area, finally building a full area mask for the sequential *Phase Unwrapping* module. The detailed procedure for *Mask Generation* is illustrated in Figure 3.

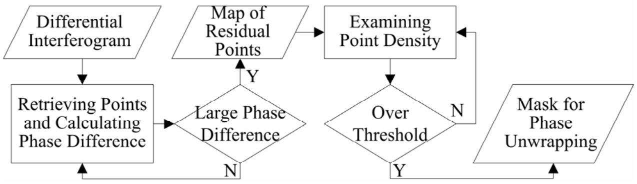

Figure 3. Detailed processes of the *Mask Generation* module

After obtaining the absolute phase values of the differential interferogram from *Phase Unwrapping*, the gradient of deformation will be computed by the *Gradient Calculation* module. Since the magnitude of gradient on the edge of deformation area are the same and larger than those in the non-deformating region, according to Attribute B, contours are then generated by the *Contours Generation* module. The gradient values on the contours can be obtained from deformation modes for specific mining areas.

The reason why contours are computed on the gradient map rather than implemented on the unwrapped interferogram directly is that, although the topographic phase has been removed from the DInSAR results, the absolute phase values still have significant differences in non-deformating areas. Take the example of phase caused by atmospheric effects [7]. It will result in the same apparent deformation values over long distances being different in DInSAR results. However, since the gradient is a relative value that represents the degree of deformation, it is impacted little by the residual phase, hence it is more suitable for generating contours.

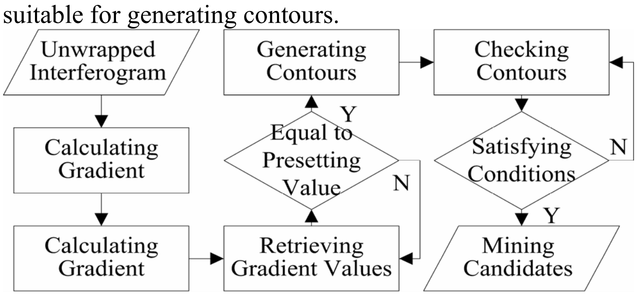

Figure 4. Detailed processes of the *Gradient Calculation* and *Contours Generation* modules

Referring to Attribute A, only subsidence patterns could be caused by underground mining, but uplifting areas can also have large magnitude gradients. Hence the contours encircle rising patterns should be disregarded. Small contours surrounded by large ones will also be removed.

Then, the regions enclosed by the remaining contours are candidates for underground mining activity locations. The operations of the *Gradient Calculation* module and the *Contours Generation* module are illustrated in Figure 4.

Correlation operations are implemented between mining candidates enclosed by selective contours and two references. The first one is a shape reference represented as an oval, which is based on Attribute C. The size and the curvature of the shape reference are determined by the target candidate. Another one, referred to as the gradient reference, is produced based on the selected contour. The gradient magnitudes are determined by the gradient of the contours. Referring to Attribute B, directions of all the gradients are perpendicular to the contour line, pointing outwards. The correlation is:

$$Cor(X,Y)=\frac{E\left\{\left[X-E(X)\right]\cdot\left[Y-E(Y)\right]\right\}}{E\left\{\left[X-E(X)\right]^2\right\}\cdot E\left\{\left[Y-E(Y)\right]^2\right\}} \tag{2}$$

where $E(\bullet)$ is the mean value operator. When shape correlation is implemented, X denotes the points on the contour line and Y denotes the shape reference. If under gradient correlation, X is the gradient of the unwrapped region that is enclosed by the contours, and Y represents the gradient reference. The final correlation coefficient used for mining detection is:

$$Cor_m = a\cdot Cor_{shape} + b\cdot Cor_{grad} \tag{3}$$

where a and b are the weighting parameters of shape correlation and gradient correlation respectively. In the following case study they are both set to 0.5. An example of these two references for a typical contour is given in Figure 5.

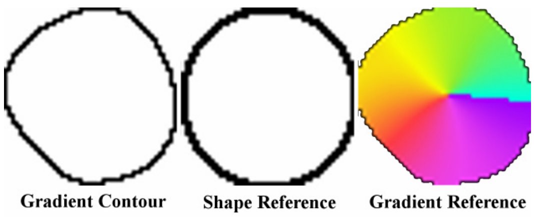

Figure 5. Example of references for a typical contour

After calculating the correlation coefficients for each mining candidates, the ones with high correlation values are then selected, confirming as mining locations. Finally, all of these detected mines are then compared with the mining plan to identify illegal mines.

3. CASE STUDY

To demonstrate the performance of the IMDS a case study of underground coal mines (including illegal ones) in Asia is examined.

The DInSAR interferogram for the mining region, is shown in Figure 6, whose coverage area is approximately 70×70 km^2. The interferogram is generated by using the two-pass DInSAR method [6] with two ALOS (Advanced Land Observing Satellite) PALSAR (Phased Array type L-band SAR) images. The master image was acquired on 15 December 2007 and the slave one was acquired on 30 January 2008. Their track and frame numbers are 453 and 72 respectively. As can be seen from Figure 6 (left), there are several areas with noise fringes, so a mask is generated based on the density of residual points to ensure a high quality unwrapped result. The mask and unwrapped interferogram are shown in Figure 6.

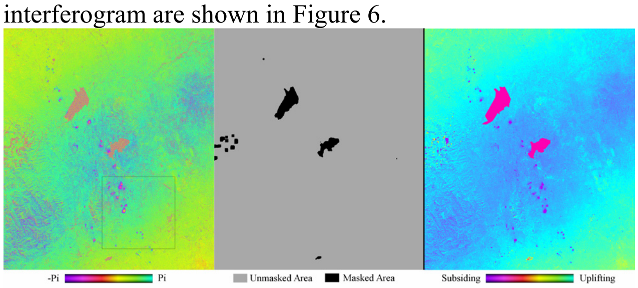

Figure 6. Differential interferogram (left), the mask for phase unwrapping (middle) and the unwrapped result (right) of selected site

After obtaining the unwrapped result, gradients are computed from it. Sequentially, contours can be obtained to aid selection of mining location candidates. In order to represent all the following processes more clearly, results are zoomed-in to the area indicated by the rectangle in Figure 6. The gradients of the zoomed-in area calculated from the unwrapped interferogram are shown in Figure 7.

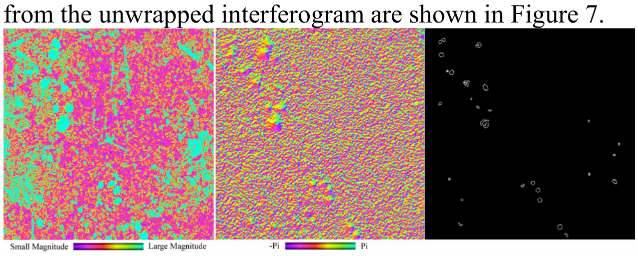

Figure 7. Magnitude (left) and phase (middle) of unwrapped result, and generated contours (right) in zoomed-in area

Contours are drawn using the gradient magnitude to determine the mining location candidates. Positions and shapes of final selected contours of the zoomed-in area are shown in Figure 7 (right image). The corresponding regions in the gradient map are mining location candidates and the correlation with shape and gradient references will be carried out. All of these contours are stored in a vector file for sequential processing. From the information in these vectors, there are 28 mining location candidates in the zoomed-in region.

The correlations are computed based on Equation (3), and values that are larger than 0.5 are considered as indicating underground mining activity. For the zoomed-in area, 17 out of 28 of the mining location candidates have been identified as mining sites (Figure 8). Finally, bu comparing these results with an official exploitation plan, the location of illegal mines can be identified.

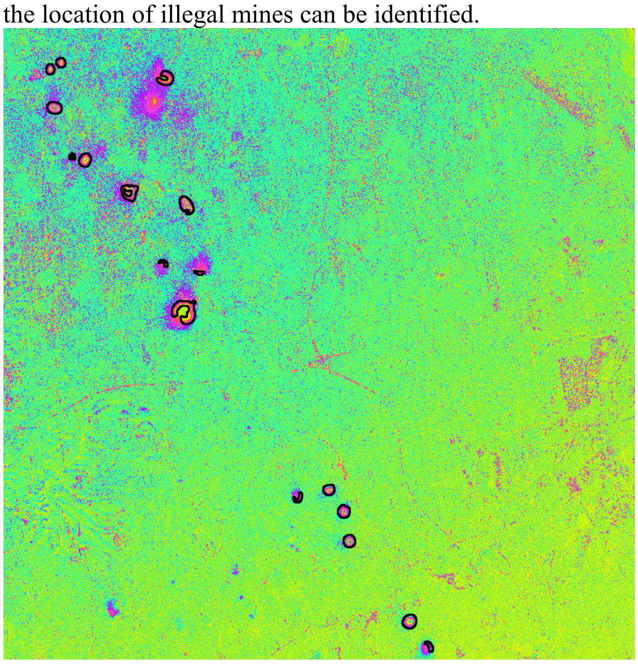

Figure 8. Detection result of underground mining

4. CONCLUDING REMARKS

In this paper the DInSAR remote sensing technique has been used to detect underground mining-induced subsidence across a large-scale area. Based on the obtained differential interferogram, an IMDS system has been proposed that increases the detection efficiency of underground mining activity. From a demonstration of its application across a region in Asia, it can be seen that most mines have been identified from the initial interferogram, and then the results are used to detect the locations of illegal mines in the region.

In future work improvements can be implemented by addressing the following problems. First of all, the detection accuracy relies on the quality of the unwrapped interferogram. Hence precise phase unwrapping algorithms are required. Secondly, the threshold of the gradient contours is currently based on processing experience and prediction of mining subsidence. If a deformation model could be developed for the mining area it could be used to define the appropriate threshold value. Moreover, correlations are implemented according to two aspects, the shape and the gradient patterns. This may be too simplistic. Ideally, a spatial 3D reference should be adopted, which will fit the characteristics of mining subsidence better.

ACKNOWLEDGEMENT

This research work has been supported by the Cooperative Research Centre for Spatial Information (CRC-SI), whose activities are funded by the Australian Commonwealth's Cooperative Research Centres Programme. The Australian Research Council and the Australian Coal Association Research Program have been funding radar related studies by the team at the University of New South Wales (UNSW) during the last few years.

The authors wish to thank the Earth Remote Sensing Data Analysis Centre (ERSDAC) for providing ALOS PALSAR data. METI and JAXA retain the ownership of the ALOS PALSAR original data. The PALSAR Level-1.1 products were produced and provided to the CRC-SI/UNSW by ERSDAC, Japan.

REFERENCES

[1]. L. Ge, H.C. Chang, C. Rizos, and M. Omura, "Mine Subsidence Monitoring: a Comparison Among Envisat, ERS, and JERS-1," *in 2004 ENVISAT Symposium*, Salzburg, Austria, Session 3P04-09, 6-10 September 2004.

[2]. U. Wegmuller, C. Werner, T. Strozzi, and A. Wiesmann, "Monitoring Mining Induced Surface Deformation," *2004 IEEE International Geoscience and Remote Sensing Symposium (IGARSS04)*, Anchorage, Alaska, Vol. 3, pp. 1933-1935, 20-24 September 2004.

[3]. C.W. Chen, and H.A. Zebker, "Phase Unwrapping for Large SAR Interferograms: Statistical Segmentation and Generalized Network Models," *IEEE Transactions on Geoscience and Remote Sensing*, Vol. 40, pp. 1709-1719, August 2002.

[4]. X. Papademetris, E. Turan Onat, A.J. Sinusas, D.P. Dione, R.T. Constable, and J.S. Dunca, "The Active Elastic Model," *Proceedings of the 17th International Conference on Information Processing in Medical Imaging*, pp. 36-49, 2001.

[5]. J. Strand, and T. Taxt, "Two-dimensional Phase Unwrapping Using Robust Derivative Estimation and Adaptive Integration," *IEEE Transactions on Image Processing*, Vol. 11, Issue 10, pp: 1192-1200, October 2002.

[6]. L. Ge, K. Zhang, A.H.M Ng, Y. Dong, H.C. Chang, and C. Rizos, "Preliminary Results of Satellite Radar Differential Interferometry for the Co-seismic Deformation of the 12 May 2008 Ms8.0 Wenchuan Earthquake," *Geographic Information Sciences*, Vol. 14, No. 1, pp. 12-19, June 2008.

[7]. L. Pipia, X. Fabregas, A. Aguasca, and C. Lopez-Martinez, "Atmospheric Artifact Compensation in Ground-Based DInSAR Applications," *IEEE Geoscience and Remote Sensing Letters*, Vol 5, Issue 1, pp. 88-92, January 2008.